2024 IEEE/RSJ International Conference on Intelligent Robots and Systems (IROS)
October 14-18, 2024. Abu Dhabi, UAE

A Perceptive Pneumatic Artificial Muscle Empowered by Double Helix Fiber Reinforcement

Yufeng Wang, Houping Wu, Chenchen Li, Yulian Peng and Hongbo Wang, *Member, IEEE*

***Abstract*— In the last decades, soft robotics has been growing rapidly as an emerging research topic, bringing new paradigms for robotic manipulation, locomotion, and human–machine interactions. Pneumatic artificial muscle is a powerful, lightweight, rapid response with great design flexibility, making it promising for developing biological muscle-like robotic systems. The PPAM is made of a silicone tube body with double helix coil fiber reinforcement. The double helix coil fiber restricts the radial expansion of the cylinder tube to achieve extension in actuation, and monitors the muscle length change in real time by measuring its inductance. A finite element model was built to simulate the actuation characteristics of the PPAM. A theoretical formula was derived to analyze the inductive length sensing response of the double-helix coil on the PPAM. It is verified that the PPAM can sense its length change regardless of whether it is caused by active driving or external manipulation. Rigorous testing reveals that PPAM has an ultrahigh length sensing resolution of 5.9 μm in relaxed state, with a short response time of 50 ms. The self-length sensing of PPAM is hysteresis free, and highly repeatable, showing no degradation in 1000 operation cycles. In summary, the PPAM shows promising features for developing the next-generation perceptive and responsive soft robots, intelligent hybrid robots, or safer biomedical instruments.**

***Keywords*— artificial muscle, proprioception, self-sensing, double helix coil, self-inductance**

I. Introduction

In the last decades, soft robotics has become a hot research field [1], [2] driven by robotics technologies and material chemistry. Compared to rigid robots, it opens new opportunities for safer human–machine interactions in a much simpler way at low cost. Among all soft actuation technologies, pneumatic actuators and robotic systems have attracted widespread attention [3], [4]. Most pneumatic actuators can be fabricated by low-cost manufacturing technologies with lightweight, hyperelastic rubber-like materials [5], [6]. Due to the flexibility and softness of pneumatic soft robots, they can actively or passively change shape to complete complex tasks efficiently. The relationship between the air pressure and deformation of pneumatic actuators has been widely studied, and the deformation trajectory of pneumatic soft robots has been derived using materials models and kinematics theory [8], [9]. Due to factors such as manufacturing errors and the complex viscoelastic behavior of these hyperelastic materials, model-based predictions of the shape changes of pneumatic soft robots are often inaccurate, making precise control of soft robots difficult. In addition, soft robots are underactuated systems with "infinite" degrees of freedom (DOFs). External loading during interactions with objects and humans can also introduce shape changes in pneumatic soft robots. To ensure closed-loop control and to achieve perceived and responsive soft robots, real-time proprioception (shape/posture perception) is crucial.

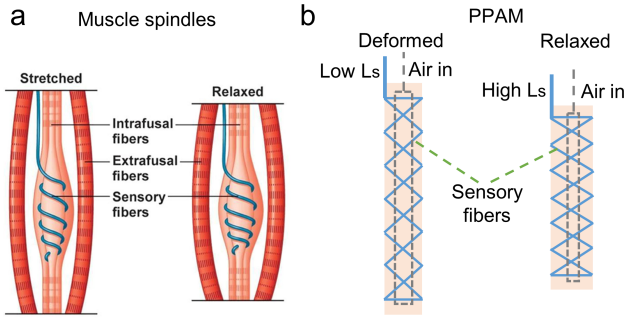

Fig. 1. (a) Illustration of muscle spindles in the stretched and relaxed states in biological systems [7]; (b) Diagrams of perceptive pneumatic artificial muscle (PPAM) in the relaxed and elongated states.

To achieve proprioception, sensors are needed to detect the strain, bending, elongation, contraction or other deformations of soft actuators and robots. To maximize the perception accuracy of pneumatic soft robots, sensors should be seamlessly integrated into pneumatic soft robots [10]. In addition, the sensor must be sufficiently compliant so that the deformations and motions of the soft robots are not affected. As summarized and discussed by Wang et al [11], researchers have studied various sensing mechanisms, from resistive, piezoresistive, capacitive, piezoelectric, optical, magnetic, to inductive sensors. Flexible and stretchable conductive materials and structures, such as liquid metal, ionic liquid/hydrogel, and nanocomposites, have been developed and applied to manufacture these sensors. In 2017, Alexander et al [12] reported an optical deformable reflective diaphragm sensor for the perception of soft robot body deformation. In 2023, Lu et al [13] reported a notable example of using a highly stretchable liquid metal strain sensor for detecting the bending of soft robots. However, to date, most of the work has focused on attaching/embedding separate sensors into the body of soft robots, which often leads to complex structures and assembly processes, impairing the sensing or actuation performance.

Recently, several studies have proposed self-sensing approaches for developing artificial muscles and soft robots

*This work was supported in part by the National Natural Science Foundation of China under Grant 52275579 and in part by the Chinese Academy of Sciences (CAS) and the University of Science and Technology of China (USTC). *(Corresponding author: Hongbo Wang.)*

The authors are with the Department of Precision Machinery and Precision Instrumentation, University of Science and Technology of China, Hefei 230026, China (e-mail: wangh@ustc.edu.cn).

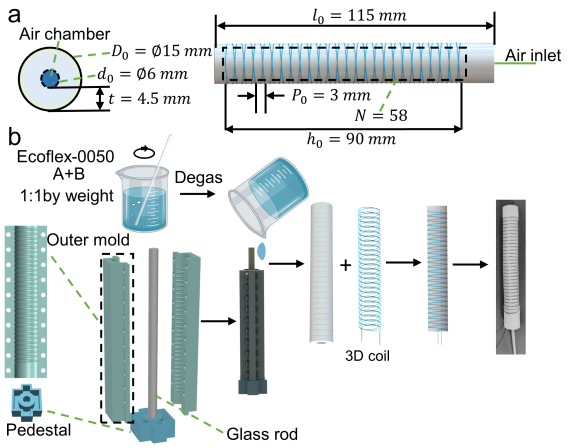

Fig. 2. Design and fabrication procedure of the PPAM: (a) Design and dimensions of the PPAM; (b) Fabrication procedure for the PPAM.

in one step. In 2016, Wakimoto et al [14] reported a conductive fiber based smart pneumatic artificial muscle, which using changes in the resistance of Ag core conductive fibers to measure the value of driving air pressure, but the perception accuracy was low. In 2018, Helps et al [15] reported a conductive working fluid based proprioceptive flexible fluidic actuator, which using the resistance variation of the conductive working fluid to measure the deformation of the actuator, however, the application of this method is limited to fluid-driven actuators, and there is hysteresis. In addition, in 2018, Truby et al [16] reported soft somatosensitive actuators via embedded 3D printing, which provides more possibilities for creating more self-sensing soft robots. In addition, in 2016, Zhao et al [17] reported a soft robotic finger with an integrated waveguide strain sensor for proprioception, however, the measurement and demodulation of waveguides are complex and inconvenient.

Inductive sensors have been widely used in industry, and start attracting interest in developing soft sensors for wearables and soft robots. In 2018, Zhou et al [18] reported a three-dimensional printed liquid metal inductive sensor capable of detecting snake like soft robots, which can accurately perceive the shape of soft robots. In addition, researchers have also developed a spring based inductive sensor that has been reported to monitor the deformation of soft robots, and the perception accuracy is high [19], [20]. From 2014 to 2018, Wyatt Felt et al proposed a "smart braid" for contraction sensing of the McKibben artificial muscle, and achieved excellent closed-loop feedback control [21], [22], [23], [24]. However, movement between the copper wires, weaving mesh, and pneumatic muscles might introduce errors in contraction sensing. And large pitch of the helical coil in "Smart Braid" would limit the contraction sensing resolution. In summary, these previous work on inductive sensors show the promising features of inductive sensing in soft robots, such as high resolution, hysteresis-free, and fast response. Fully integrated sensing and actuation in one body is highly desirable for developing high performance perceptive soft robots.

In biological systems, muscle spindles (Fig. 1a) provide contraction information via sensory fiber wounds on intrafusal fibers, which enables proprioception of joint angles and external interaction forces. Inspired by this biological system, we present a perceptive pneumatic artificial muscle (PPAM), which is made of a cylindrical silicone tube reinforced by a double-helix conductive fiber (Fig. 1b). As the inextensible double-helix conductive fiber restricts its radial expansion, the PPAM elongates when high pressure is applied to its inner chamber. On the other hand, the double-helix conductive fiber forms a helical shape inductive coil similar to a mechanical spring, and the inductance of this double-helix fiber coil decreases with the elongation of the PPAM. Therefore, real-time elongation of the PPAM can be monitored by measuring the inductance of the double-helix coil.

II. PPAM Design and Fabrication

As shown in Fig. 2a-b, the PPAM is a cylindrical tube with an outer diameter of 15 mm, and an inner diameter of 6 mm. One end of the tube was encapsulated, and the other end was sealed with a silicone tube as an air inlet to connect the pneumatic driving system. The double-helix fiber has an initial pitch of 3 mm for the helical coil, with 58 turns in total (29 turns for each helical coil). All parameters of the PPAM are listed in Tab. 1.

Table 1. Design parameters of the PPAM

Parameters	*Symbol*	*Value*	*Unit*
Length	l_0	115	mm
PPAM outside diameter	D_0	15	mm
Air chamber diameter	d_0	6	mm
Number of coil winding turns	N	58	/
The initial pitch of the coil	P_0	3	mm
Wall thickness	t	4.5	mm
The height of coil	h_0	90	mm

To fabricate the PPAM, two parts of the outer molds were 3D printed using photopolymer resin (FLGPWH04, Formlabs, USA) via a stereolithography (SLA) 3D printer (Formlabs Form2), to obtain fine details of the double-helix pattern at the inner surface. A glass rod was used as an inner support to form the air chamber. As depicted in Fig. 2b, the outer molds were assembled and fixed by screw bolts, and mounted on a pedestal together with the glass rod. To obtain the PPAM body, parts A and B of Ecoflex-0050 (Smooth-On, PA, USA) were mixed (1:1 by weight) and degassed, then poured into the mold slowly and cured at room temperature. After demolding, a silicone tube with one end encapsulated and grooves of the double-helix path on its outer surface is obtained. Next, a conductive fiber (multithread electrical wire with Teflon sheath, FF46-2-19/0.04 mm, OD: 0.3 mm) was wound on the outer surface of the silicone tube by carefully following one helical groove (clockwise) from one end to the other, and then wound back to the starting point by following the other helical groove (counterclockwise). Then, a thin layer of uncured silicone was evenly brushed on the surface to fix the conductive fibers. Finally, the open end was inserted with a silicone tube as the air inlet end and sealed with silicone adhesive (ELASTOSIL E41, WACKER, Germany).

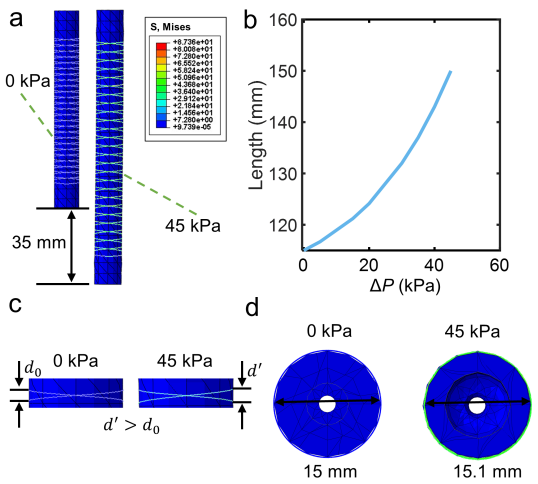

Fig. 3. Finite element simulation of the PPAM: (a) Stress cloud map of the PPAM at 0 kPa and 45 kPa; (b) Length of the PPAM at a driving pressure from 0 to 45 kPa; (c) Magnified view of the helical coil expansion at 45 kPa with respect to 0 kPa; (d) Cross-sectional morphology of the PPAM at 0 kPa and 45 kPa.

III. FEM OF ACUTATION

A finite element (FE) model of the PPAM was developed in Abaqus/Standard. In the FE model, the elastic body (enclosed silicone tube) is created as a three-dimensional (3D) entity and the double helix coil is created as a 3D line. First, the Yeoh hyperelastic material model [25] was used to simulate the nonlinear behavior of the silicone material. The strain energy is

$$U = \sum_{i=1}^{3} C_i (I_1 - 3) \tag{1}$$

where U is the strain energy, C_i is the material parameter, and I_1 is the first invariant of the Cauchy–Green strain tensor. The coefficients used for Ecoflex-0050 are C_1=1.9×10^{-2} MPa, C_2=9×10^{-4} MPa and C_3=-4.75×10^{-6} MPa [26]. The double helix coil wire was modeled as a linear elastic material (Young's modulus of E = 119 GPa and Poisson's ratio of v = 0.326). The boundary between the silicone tube and the double helix coil is defined as a tie connection. The elastic body was meshed in solid tetrahedral quadratic hybrid elements (Abaqus element type C3D10H), while the coil fiber was meshed in quadratic beam elements (Abaqus element type B32H). Air pressure is applied on the whole cylindrical inner surface of the PPAM air chamber.

As shown in Fig. 3a, the simulated stress cloud map of the PPAM at 45 kPa shows that the stress during actual operation is mainly concentrated on the coil fiber. The length of the PPAM increases with increasing applied pressure (Fig. 3b). A cross-sectional view of the PPAM (Fig. 3c and Fig. 3d) confirms that the radial expansion of the PPAM is only 0.1 mm (0.6%) due to the restriction of the double helix fibers. As expected, the helical coil fiber elongated along its axis with the extended silicone body.

IV. THEORETICAL ANALYSIS OF THE LENGTH SENSING

As illustrated in Fig. 4a, the double helix coil is composed of two single helix coils connected in series. One helix coil is clockwise, and the other is counterclockwise, ensuring the same current flow direction and positive mutual inductance. On the other hand, the double helix coil design also ensures pure elongation deformation of the PPAM without twisting or bending. To derive the theoretical inductance equation under deformation, a simplified single helix model was used. According to Wheeler's formula [27], the inductance of a helical coil (solenoid) can be calculated as

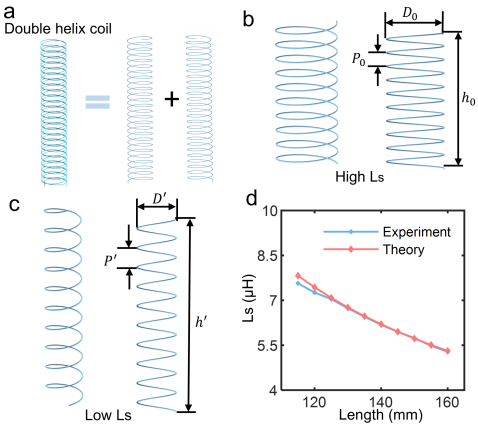

Fig. 4. The inductive sensing principle of PPAM: (a) Composition of the double helix coil; (b) Dimensions of the single helical coil at null deformation; (c) Dimensions of the extended single helical coil; (d) Comparison of the theoretical calculation and experimental results of the inductance response to the PPAM length.

$$L_{s0} = \frac{N^2 {D_0}^2}{450 D_0 + 1000 h_0} \tag{2}$$

where N is the number of turns, D_0 is the diameter of the initial state, and h_0 is the height of the initial state. The units of D_0 and h_0 are mm, and the calculated inductance is μH. Considering that the 3D helical coil was embedded in the soft body, it extends along the axis with the PPAM body. At the same time, the helical coil contracts radially as the total length of the coil fiber becomes inextensible. To accurately calculate the inductance of the coil when the PPAM is elongated. The total conductive fiber length s_0 at the initial state is

$$s_0 = \sqrt{(N\pi D_0)^2 + {h_0}^2} \tag{3}$$

As shown in Fig. 4c, when the PPAM was extended, the pitch of the coil increased, and the diameter decreased. Since the total length of the coil fiber is inextensible (the Young's modulus of fibers is much greater than the deformation stress), the parameters of the extended helical coil are as follows

$$s' = \sqrt{(N\pi D')^2 + h'^2} = s_0 = \sqrt{(N\pi D_0)^2 + {h_0}^2} \tag{4}$$

Therefore, the diameter D' of the extended coil can be calculated as

$$D' = \sqrt{(N\pi D_0)^2 + h_0^2 - h'^2} \tag{5}$$

The inductance L'_s of the extended coil can be calculated as

$$L'_s = \frac{N^2((N\pi D_0)^2 + h_0^2 - h'^2)}{450\sqrt{(N\pi D_0)^2 + h_0^2 - h'^2} + 1000h'} \tag{6}$$

Since radial contraction of the helical coil is taken into account in the above derivation, the accurate inductance of the PPAM can be calculated even for very large deformations. Fig. 4d shows that the calculated inductance matches well with the experimental results. It should be noted that the length of PPAM shown in Fig. 4d equals the length of the helical coil plus the length of the two ends (as illustrated in Fig. 2b).

V. Results and Discussion

A. Experimental Setup

To characterize the response of the PPAM to actuation and sensing, and evaluate its performance under various conditions, a pneumatic drive system was developed. As illustrated in Fig. 5, a syringe pump setup was developed to drive the PPAM at a specific pressure. The real-time pressure was monitored with a commercial pressure sensor (ASDXRRX030PGAA5, Honeywell, USA) with an ADC board (NI USB 6210, TX, USA), while the inductance was measured with a circuit board which had an inductance measurement chip LDC1614. A laser sensor (HG-C1200-P, Panasonic, Japan) was attached in parallel with the PPAM to read its length change. A LabView-based program was developed for air pressure data and inductance data acquisition, as well as for controlling the motorized linear stages to drive the syringe pump for pressure regulation.

B. Characterization of the PPAM

First, the self-sensing and actuation functions of the PPAM are verified. Fig. 6a shows images of the PPAM prototype at driving pressures of 0 kPa, 28 kPa and 40 kPa with a scale indicating its length. The magnified images highlight the increased pitch of the double-helix coil when the driving pressure of the PPAM increased to 40 kPa. To characterize its actuation function, the PPAM was pressurized to 45 kPa and depressurized, and the air pressure and length were recorded. Fig. 6b shows a length-to-pressure curve similar to that of the simulation results in Fig. 3b, with a maximum elongation of 50 mm (43%) at 45 kPa. Notably, there is a clear hysteresis of 10.2% between the length and the applied pressure during the elongation-relation cycle, which is one of the main reasons that PPAM deformation cannot be precisely controlled via open-loop control of the air pressure. In addition, the actuation curve can be significantly affected by the dynamics of the pneumatic driving system and the relaxation and creep effects of the silicone materials. Fig. 6c shows that the inductance of the double helix coil decreased

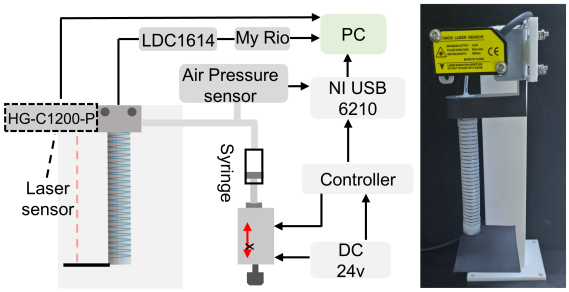

Fig. 5. Experimental setup for the sensing and actuation characterization of the PPAM.

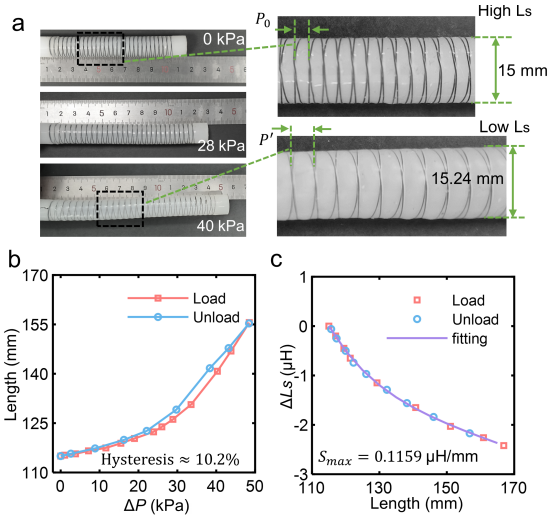

Fig. 6. Actuation and self-sensing characteristics of the PPAM. (a) Photographs of the PPAM under driving pressures of 0 kPa, 28 kPa and 40 kPa with magnified view to highlight the pitch change of the double helix coil; (b) Length change of the PPAM during a load and unloading cycle; (c) Inductance of the double-helix coil decreases with elongation of the PPAM.

with increasing PPAM length, as predicted by theoretical analysis. The two inductance-to-length curves during pressurization and depressurization completely overlap, without any hysteresis, guaranteeing precise length control via sensor feedback. Fig. 6c also shows that the inductance of the double helix coil decreased by 2.42 μH when the PPAM length increased to 165 mm from its original length of 115 mm. The curve fitting result indicates that the variation in the inductance with respect to the deformation matches well with an exponential function, with R^2 = 0.99. The sensitivity decreases from 0.1159 μH/mm at 115 mm length to 0.0249 μH/mm at 165 mm length.

C. Perception of active and passive deformation

As discussed in the introduction, the PPAM can detect any deformation (length change) regardless of its cause, making it a good candidate for feedback control and interaction with the external environment. Fig. 7a plots the changes in the recorded air pressure and inductance during four pressurization–depressurization cycles and an incremental pressurization–depressurization test. The curve shows that the PPAM can perceive its length change in real time under dynamically changing driving pressure. When the PPAM was manually pulled to extend, the measured inductance responded spontaneously (Fig. 7b) to the length change, while the monitored pressure varied within a very small range of less than 1 kPa. In addition, when the PPAM was pulled by weight hanging below to extend, the measured inductance also responded spontaneously (Fig. 7c) to the length change, while the monitored pressure varied within a very small range of less than 0.3 kPa. Thus, the air pressure change cannot reflect the true deformation of the PPAM during interaction. This test highlights that the PPAM's inductance can provide a reliable, fast response and stable measurement of its length, as Fig. 7b and Fig. 7c indicate that the inductance variation returns to zero once the muscle is relaxed to its original state.

D. Performance evaluation of the PPAM

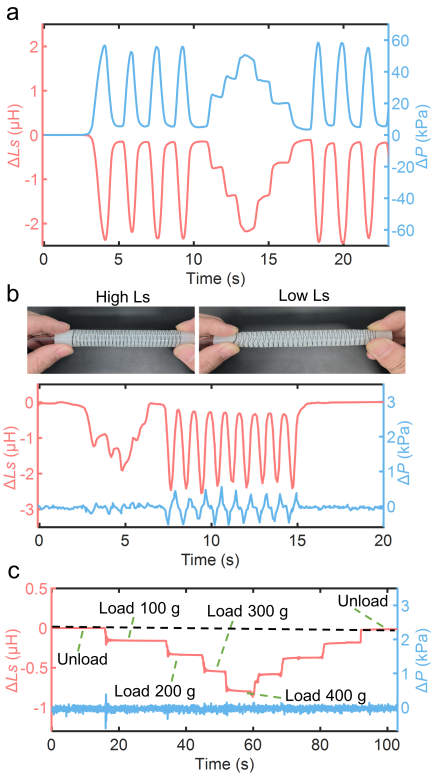

Fig. 7. The sensing response of PPAM under (a) active driving, (b) passive deformation introduced by manual pulling and (c) passive deformation introduced by weight hanging below.

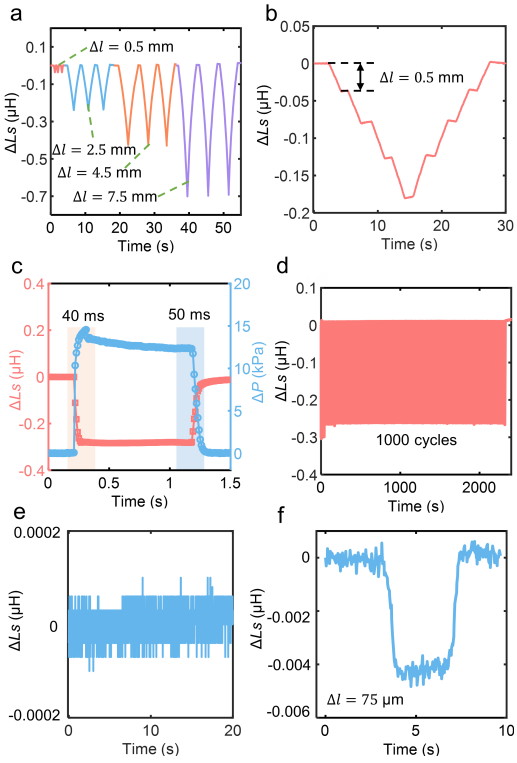

Fig. 8. Characterization of the PPAM performance. (a) Inductance response of PPAM under three cycles of pressurization and depressurization at different driving pressures; (b) Inductance response of PPAM under a small incremental pressure to achieve an elongation step of 0.5 mm; (c) Real-time response of PPAM under an on-off pressure; (d) 1000 cycles of testing the long-term stability of PPAM. (e) The inductance measurement noise; (f) Inductance response of PPAM with 75 μm elongation driven by a very small air pressure (0.3 kPa).

As discussed above, the PPAM seamlessly combines actuation and sensing. To evaluate the repeatability of the PPAM at different deformations, the PPAM was pressurized and depressurized for three cycles at four different air pressures (Fig. 8a). Fig. 8a shows that the PPAM can work repeatedly under different deformations, and the corresponding inductance variations have good repeatability. As shown in Fig. 8b, the PPAM was driven by a small pressure to achieve an incremental length change with a step of 0.5 mm. The corresponding inductance variation is approximately 0.044 μH for each step. Fig. 8b also indicates that the PPAM can be controlled to perform stable and accurate deformation movements. Then, an on-off pressure (12.8 kPa) was applied to the PPAM via a valve to evaluate its response time. The results (Fig. 8c) show that the inductance responds simultaneously with applied pressure, indicating a short response time of 50 ms for elongation and 40 ms for recovery. This rapid response for both actuation and sensing indicates an operating frequency of 11 Hz, which matches the performance of human muscles [28]. In addition, the PPAM was subjected to a 13 kPa on-off pressure for 1000 cycles at a frequency of 0.43 Hz, and the results (Fig. 8d) highlight the excellent stability of the PPAM, which is a promising feature for long-term operation in practical applications.

To evaluate the deformation sensing resolution of the PPAM, a 40 s inductance was recorded at a sampling rate of 100 Hz (Fig. 8e), indicating a measurement noise (RMS) as low as 3×10^{-5} μH. Thus, the deformation sensing resolution of the PPAM is 5.9 μm at null deformation. In contrast to most soft actuators, the PPAM can achieve extremely fine deformation control down to tens of micrometers. Fig. 8f shows that the PPAM was driven by an extremely small pressure (0.3 kPa) that caused a deformation of 75 μm, and the inductance signal clearly detected such a small elongation.

E. PPAM-based soft robotic systems

Although PPAM only has one mode of actuation, elongation, multiple PPAMs can be bundled to achieve multi-DOF deformation to perform specific tasks. For instance, the snake or octopus tentacle-inspired continuum robot (either for manipulation or locomotion) can be developed by configuring PPAMs as bundles to achieve deformation in a specific direction. Fig. 9 shows the preliminary test of the PPAM bundles for bidirectional and omnidirectional bending. As shown in Fig. 9a, two PPAMs were bonded together to achieve two working modes of bidirectional bending and elongation. When the left PPAM is pressurized, the soft actuator bends to the right, and vice versa. When both PPAMs are pressurized, the soft actuator elongates. Fig. 9b shows a soft robot arm capable of omnidirectional bending in 3D space by controlling the driving pressures of the triple-PPAM. In the future, we will further optimize the PPAM and develop intelligent soft arm and locomotion robots using PPAM modules and other self-sensing pneumatic actuators. By exploiting high-resolution, seamlessly integrated sensing data, next-generation soft robots can perceive their own body shape and environment, allowing active adaptation, interaction, response and exploration of their surroundings, similar to biological creatures.

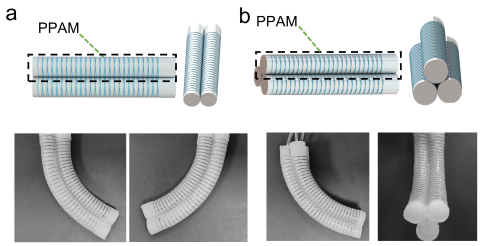

Fig. 9. Development of the PPAM-based soft robotic system. (a) Configuration and images of the Two-PPAM-based bundle for bidirectional bending; (c) Configuration and images of the triple-PPAM bundle for omnidirectional bending and elongation.

VI. Conclusion

In this paper, we proposed a perceptive pneumatic artificial muscle (PPAM). The double helix fiber reinforcement ensures linear extension along its axis of the PPAM when it is pressurized. Length of the PPAM can be monitored by measuring the inductance of the double-helix coil. We performed finite element simulation and theoretical formula derivation to investigate its actuation and sensing characteristics. PPAM prototypes were developed and characterized. It can perceive both length changes due to internal driving or external stimuli. The PPAM achieved motion and sensing responses within 50 ms, indicating an operation frequency of 11 Hz (comparable to human muscles). And both sensing and actuation can operate repeatedly without any degradation in 1000 cycles of elongation and recovery. Experimental results show the PPAM can perceive extremely small length changes with a sensing resolution of 5.9 μm without hysteresis. More importantly, the PPAM can be building blocks to be assembled in different configurations to perform meaningful manipulation or locomotion tasks.

In the near future, we will focus on developing closed-loop feedback control and environmental interactions with PPAMs. By configuring multiple PPAMs in a bundle, soft robotics systems (e.g., crawling robots, continuum soft robotic arms, or soft grippers) can be developed to achieve complex biomimetic behaviors or fine movement/manipulation skills with sensing-data-driven control.

References

[1] C. Majidi, "Soft robotics: a perspective—current trends and prospects for the future," Soft robotics, vol. 1, no. 1, pp. 5-11, 2014.

[2] S. Bauer, S. Bauer-Gogonea, I. Graz, M. Kaltenbrunner, C. Keplinger, and R. Schwödiauer, "25th anniversary article: a soft future: from robots and sensor skin to energy harvesters," Advanced Materials, vol. 26, no. 1, pp. 149-162, 2014.

[3] J. Walker et al., "Soft robotics: A review of recent developments of pneumatic soft actuators," in Actuators, 2020, vol. 9, no. 1: MDPI, p. 3.

[4] H. Su et al., "Pneumatic soft robots: Challenges and benefits," in Actuators, 2022, vol. 11, no. 3: MDPI, p. 92.

[5] N. Gariya and P. Kumar, "A review on soft materials utilized for the manufacturing of soft robots," Materials Today: Proceedings, vol. 46, pp. 11177-11181, 2021.

[6] F. Schmitt, O. Piccin, L. Barbé, and B. Bayle, "Soft robots manufacturing: A review," Frontiers in Robotics and AI, vol. 5, p. 84, 2018.

[7] Tom Myers, "Q&A with Tom: Spindles and GTO's: Explaining the Gamma System," https://www.anatomytrains.com/blog/2014/02/17/spindles-gtos, 2014.

[8] N. An, M. Li, and J. Zhou, "Modeling and understanding locomotion of pneumatic soft robots," Soft Materials, vol. 16, no. 3, pp. 151-159, 2018.

[9] M. S. Xavier et al., "Soft pneumatic actuators: A review of design, fabrication, modeling, sensing, control and applications," IEEE Access, vol. 10, pp. 59442-59485, 2022.

[10] C. Hegde, J. Su, J. M. R. Tan, K. He, X. Chen, and S. Magdassi, "Sensing in soft robotics," ACS nano, vol. 17, no. 16, pp. 15277-15307, 2023.

[11] H. Wang, M. Totaro, and L. Beccai, "Toward perceptive soft robots: Progress and challenges," Advanced Science, vol. 5, no. 9, p. 1800541, 2018.

[12] A. M. Hart, L. O. Tiziani, J. H. Jung, and F. L. Hammond, "Deformable reflective diaphragm sensors for control of soft pneumatically actuated devices," in 2018 IEEE International Conference on Soft Robotics (RoboSoft), 2018: IEEE, pp. 132-139.

[13] S. Lu, J. Jiao, X. Li, H. Wang, H. Wu, and Q. Li, "An Ultrawide Range, Highly Stretchable Liquid Metal Force and Strain Sensor Based on Spiral Multilayer Microfluidic Fibers," IEEE Transactions on Industrial Informatics, 2023.

[14] S. Wakimoto, J. Misumi, and K. Suzumori, "New concept and fundamental experiments of a smart pneumatic artificial muscle with a conductive fiber," Sensors and Actuators A: Physical, vol. 250, pp. 48-54, 2016.

[15] "Proprioceptive Flexible Fluidic Actuators Using Conductive Working Fluids," Soft Robotics, vol. 5, no. 2, pp. 175-189, 2018, doi: 10.1089/soro.2017.0012.

[16] R. L. Truby et al., "Soft Somatosensitive Actuators via Embedded 3D Printing," Advanced Materials, vol. 30, no. 15, p. 1706383, 2018, doi: https://doi.org/10.1002/adma.201706383.

[17] H. Zhao, K. O'Brien, S. Li, and R. F. Shepherd, "Optoelectronically innervated soft prosthetic hand via stretchable optical waveguides," Science Robotics, vol.1, no.1, peaai7529, 2016, doi:10.1126/scirobotics. aai7529.

[18] L.-Y. Zhou, Q. Gao, J.-F. Zhan, C.-Q. Xie, J.-Z. Fu, and Y. He, "Three-dimensional printed wearable sensors with liquid metals for detecting the pose of snakelike soft robots," ACS applied materials & interfaces, vol. 10, no. 27, pp. 23208-23217, 2018.

[19] S. K. Sahu, I. Tamadon, B. Rosa, P. Renaud, and A. Menciassi, "A Spring-Based Inductive Sensor for Soft and Flexible Robots," IEEE Sensors Journal, vol. 22, no. 20, pp. 19931-19940, 2022.

[20] Y. Cho, W. Kim, H. Park, J. Kim, and Y. Na, "Bidirectional Double-Spring Pneumatic Artificial Muscle With Inductive Self-Sensing," IEEE Robotics and Automation Letters, 2023.

[21] W. Felt and C. D. Remy, "Smart braid: Air muscles that measure force and displacement," in 2014 IEEE/RSJ International Conference on Intelligent Robots and Systems, 2014: IEEE, pp. 2821-2826.

[22] W. Felt, K. Y. Chin, and C. D. Remy, "Contraction sensing with smart braid McKibben muscles," IEEE/ASME Transactions on Mechatronics, vol. 21, no. 3, pp. 1201-1209, 2015.

[23] W. Felt, K. Y. Chin, and C. D. Remy, "Smart braid feedback for the closed-loop control of soft robotic systems," Soft robotics, vol. 4, no. 3, pp. 261-273, 2017.

[24] W. Felt, S. Lu, and C. D. Remy, "Modeling and design of "smart braid" inductance sensors for fiber-reinforced elastomeric enclosures," IEEE Sensors Journal, vol. 18, no. 7, pp. 2827-2835, 2018.

[25] O. H. Yeoh, "Some forms of the strain energy function for rubber," Rubber Chemistry and technology, vol. 66, no. 5, pp. 754-771, 1993.

[26] M. S. Xavier, A. J. Fleming, and Y. K. Yong, "Finite element modeling of soft fluidic actuators: Overview and recent developments," *Advanced Intelligent Systems,* vol. 3, no. 2, p. 2000187, 2021.

[27] H. A. Wheeler, "Simple inductance formulas for radio coils," Proceedings of the institute of Radio Engineers, vol. 16, no. 10, pp. 1398-1400, 1928.

[28] S. Schiaffino and C. Reggiani, "FIBER TYPES IN MAMMALIAN SKELETAL MUSCLES," *Physiological Reviews,* vol. 91, no. 4, pp. 1447-1531, Oct 2011, doi: 10.1152/physrev.00031.2010.